Journal of Fluid Science and Technology

Vol. 6, No. 3, 2011

Experimental and Numerical Studies on a Low Reynolds Number Airfoil for Wind Turbine Blades*

M. Rafiuddin AHMED**, Sumesh NARAYAN**, M. Asid ZULLAH*** and Young-Ho LEE***

**Division of Mechanical Engineering, The University of the South Pacific
Laucala Campus, Suva, Fiji

***Division of Mechanical and Information Engineering, Korea Maritime University
1 Dongsam-dong Youngdo-Ku, Busan 606-791, Korea
Email: lyh@hhu.ac.kr

Abstract

Testing of a low Reynolds number airfoil designed for low speed horizontal axis wind turbine (HAWT) blades was performed to study its aerodynamic characteristics. Experiments were conducted at Reynolds numbers (Re) of 38,000 to 200,000 at angles of attack from -2^o to 20^o. The airfoil geometry was chosen after testing a number of profiles with XFOIL software. The pressure distribution, lift and drag coefficients and the flow characteristics were also studied with ANSYS-CFX software. The freestream turbulence level was increased from 1% to 5% and 10% which shifted the transition point on the upper surface upstream, resulting in increased skin friction drag for lower angles of attack due to a larger turbulent boundary layer region. The slope of the lift curve did not change much at higher turbulence levels; however, for higher angles of attack, the separation from the upper surface was delayed resulting in an increase in lift and a reduction in drag. The lift to drag ratio increased by 8% to 15% as a result of increasing the turbulence level in the angles of attack-range of interest.

Key words: Low Reynolds Number Airfoil, Pressure Distribution, Lift, Drag, Wind Turbine, Turbulence Intensity

1. Introduction

The commonly used NACA airfoils are not appropriate for wind turbines that need to operate in regions of low wind. The NACA airfoils are suitable for applications where the Reynolds numbers (Re) are high and the angles of attack are relatively small [1,2]. Attempts are being made to develop good airfoil geometries that are appropriate at low Re for energy extraction from the wind at low wind speeds. The rotor blade is one of the most important parts of the wind turbine which is the primary energy conversion device. For the wind turbine blade design, the selection of airfoils for different sections and the distribution of chords and twists are pivotal [3].

Research efforts directed at maximizing the power output of wind turbines have increased significantly during the recent years. A number of sites in many countries have locations where the wind speeds are not very high. As the aerodynamic efficiency increases with tip speed, advances in the development of small wind turbines will provide solutions to the energy requirements of many countries. Researchers have been trying to make performance data sets of representative airfoils available, which will help in validating

*Received 27 Oct., 2010 (No. 10-0494)
[DOI: 10.1299/jfst.6.357]

prediction codes used for design purposes [4,5]. The present investigation is a part of the work undertaken to study the performance characteristics of a few airfoils that are suitable for low Re applications, and then use the knowledge gained during the process to design our own airfoils for specific applications. In the present work, a number of existing airfoil geometries were tested with XFOIL software [6]. Based on the performance of these airfoils over a range of low Re and angles of attack (α), the profile SG6043 [7] was chosen for experimental and computational analysis. This profile has been tested in the past; however, there is a wide scatter in the results available for this airfoil in open literature. For example, the stall angle reported in one of the databases is 10.5^o for Re = 100,000 [8], while some researchers have reported stalling at about 15^o for this Re. The shape of the profile indicates that it is a good compromise between the NACA airfoils and the highly cambered very low Re airfoils [2].

The present work is aimed at gaining a deeper insight into the flow characteristics and the lift and drag behavior of SG6043 at different low Re and α, to assess its appropriateness for applications in wind turbines suitable for the wind speeds of 4-6 m/s that are common in the Pacific Island Countries. The power requirements in the Pacific Island Countries are not large, with many individual islands requiring only a few hundred kiloWatts. The Pacific Island Countries have small populations which are scattered, especially on small islands. This means that small wind turbines of the order of 10-20 m diameters will be able to meet the requirements of many of the villages located on these islands. For applications of this type, it is essential to study the airfoil characteristics at low Re. In this work, the Re, α and freestream turbulence levels (Tu) were varied to study their influence on the aerodynamic characteristics of the airfoil. The Re was varied from 38,000 to 200,000 which corresponds to the region from the hub to about 70% of the distance towards the tip. Most of the contribution to the lift force comes from the region slightly inboard from the tip where the Re is of the order of 150,000-200,000 for smaller turbines under consideration for a tip speed ratio of about 5 and normal rotational speeds. The attention of the study is focused on angles of attack up to 20^o. In most cases, it is desirable that the design α-region is close to the maximum value of lift coefficient ($C_{l,max}$).

The freestream turbulence level was varied from the normal value of 1% to study its effect on the airfoil performance. A few cases were studied for the freestream turbulence levels of 5% and 10%. The freestream turbulence levels of the atmospheric wind at heights at which wind turbines are normally installed are generally higher compared to the levels achieved in standard wind tunnels. It is known that the airfoil characteristics change with freestream turbulence level [9-13]. Hoffmann [9] studied the effect of varying the freestream turbulence intensity from 0.25% to 9% for NACA0015 airfoil at Re = 250,000 and reported an increase in the peak lift coefficient due to delayed flow separation at higher angles of attack. Swalwell et al. [10] varied the freestream level from 0.6% to 7% and studied the pressure distribution and lift and drag characteristics for NACA0021 airfoil. Devinant et al. [11] varied the turbulence level from 0.5% to 16% and studied its effect on NACA 65_4-421; they found that the flow was separating at higher angles of attack when the turbulence level was increased. Recently Maeda et al. [12] studied the effects of turbulence intensity on the static and dynamic characteristics of DU93-W-210 airfoil at Re = 350,000 at two turbulence levels of 0.15% and 11%. They observed the hysteresis loop at the low turbulence level of 0.15%, which reduced at higher turbulence levels. They also found that the flow separation gets delayed at higher turbulence levels and the stall angle gets increased. Sicot et al. [13] varied the turbulence level from 4.4% to 12% and studied the effect on the lift, drag and power output characteristics of a NACA65_4-421 profiled blade. Thus, it can be seen that most of the works on such studies are done on NACA airfoils. Based on the above-mentioned works and their findings and the fact that the turbulence levels at lower altitudes and in the wake of other wind turbines (for wind farm applications)

varies in this range [14], it was decided to investigate the effect of turbulence levels by also studying the airfoil characteristics at 5% and 10%.

With a sudden change in the turbulence level of the wind, the flow structure over the blade changes significantly, shifting the location of transition as well as that of separation. Therefore, it is advisable to choose a profile that has the upper surface transition point very close to the leading edge at the design angle of attack. This paper presents the results from a detailed study, in which the performance characteristics of a low Re airfoil are studied at different freestream turbulence levels, both experimentally and numerically and attention is focused on α and Re values which are appropriate as design points.

Nomenclature

A	airfoil planform area = c × span [m^2]
c	chord length [m]
C_l	coefficient of lift = $L/q_\infty A$
C_d	coefficient of drag = $D/q_\infty A$
Cp	coefficient of pressure = $(p - p_\infty)/q_\infty A$
D	drag force [N]
L	lift force [N]
p	static pressure at a point [N/m^2]
p_∞	freestream static pressure [N/m^2]
q_∞	freestream dynamic pressure [N/m^2]
Re	Reynolds number = $\rho U_\infty c/\mu$
Tu	turbulence intensity = $\sqrt{0.5(\overline{u'^2} + \overline{v'^2})}/U_\infty$ [%]
u’	fluctuation in streamwise velocity [m/s]
v’	fluctuation in transverse velocity [m/s]
U_∞	freestream mean velocity [m/s]
x	distance along chord from the leading edge [m]
x_{tr}	distance along chord where transition occurs [m]
α	angle of attack [degrees]
μ	dynamic viscosity [$N.s/m^2$]
ρ	air density [kg/m^3]

2. Experimental Method

2.1 Wind tunnel and Airfoil

The experiments were carried out at four different velocities in an open circuit, suction type, low-speed wind tunnel. The air flow in the tunnel was generated by a single stage centrifugal flow fan having a rated discharge of 4.53 m^3/s at the pressure head of 996.7 Pa and the speed of 2253 rpm. The fan is driven by a thyristor controlled 10 HP AC motor. A settling chamber, provided with honeycomb gauges and three high-porosity screens, was used for correcting the flow. A bell-mouthed inlet section ensured smooth entry of the air to the settling chamber. The airflow was discharged into the test section through the square outlet of the contraction. The area ratio of the contraction nozzle is 6.25:1. A smooth variation in velocity from 3 m/s to 50 m/s can be achieved in the test section having dimensions of 303 mm x 303 mm x 1000 mm. The test section is provided with perspex windows on both sides. A traversing mechanism is provided on top of the test section for moving the pitot-static tube and hot-wire anemometer probe along its length in the mid-span plane of the airfoil. The freestream turbulence intensity in the test section was found to be about 0.8% at the highest velocity and was of the order of 1% in the Re range of interest.

Measurements of surface pressures were carried out with the help of a Furness Controls Micromanometer (model FCO510) having a range of ±19620 Pa. The Micromanometer was calibrated against a U-tube water manometer. The lift and drag forces were measured with a dynamometer. The low Re SG6043 airfoil, investigated in the present work, has a maximum thickness of 10%, a camber of 5.5% and a leading edge radius of 1.7%. The profile is shown in Fig. 1. It was made out of wood in the laboratory. Thirty four pressure taps were provided on the upper and lower surfaces of the airfoil to measure the pressure distribution. The chord length of the airfoil (c) was 100 mm.

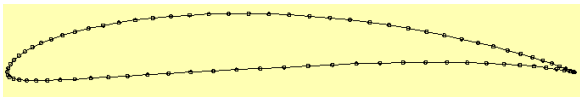

Fig. 1. Geometry of the airfoil.

2.2 Experimental procedure

The mean velocity was set with the help of the thyristor system. Experiments were carried out at four Re of 38,000, 100,000, 150,000 and 200,000 based on the chord length and the corrected freestream velocity. The freestream velocity was corrected for blockage [15] and the thyristor system frequency was obtained for the required Re values at different values of α. The constant chord length blade (henceforth, it will be called the test model) was placed horizontally in the test section and it spanned the width of the test section. The axial location of the leading edge was only 10 cm from the exit of the contraction. In view of this, the very small flow component towards mid-span due to the boundary layer on the side walls of the test section does not affect our pressure measurements as the pressure taps were provided near the mid-span of the test model, thus providing a two-dimensional flow over the pressure taps (airfoil characteristics). Another airfoil with a slightly shorter span was used for making lift and drag measurements. The angle of attack was varied from -2^{o} to 20^{o} and the pressure measurements were performed. The freestream turbulence level was varied by changing the turbulence screens before the contraction and the scale of turbulence was smaller compared to the chord length of the airfoil. The pressures were converted to the pressure coefficient (C_P). The accuracy of C_P measurements was estimated to be 1.72%, while the repeatability was 1.55%.

3. Computational Method

The airfoil geometry was imported into the pre-processor. The domain was chosen such that a minimum distance of 15 times the chord length of the airfoil was maintained from the airfoil to the edges. The airfoil was located in the middle of domain. The geometry was meshed using the software ICEM CFD. The mesh is based on structured O-grid and C-grid topology and properly resolves the boundary layer, the size of cells adjacent to the walls is limited by $y+ < 1$. The resulting size of the mesh is 1210600 nodes. The meshing around the airfoil is shown in Fig. 2. Turbulent flow solution was used in ANSYS CFX and the turbulence modeling was done with κ-ω based SST model. The transition modeling was done with 'Gamma Theta Model'. The inlet velocity was varied to get the desired Re based on the airfoil chord length. The freestream turbulence level of the incoming air was set at 1%, 5% and 10% to study the effect of turbulence intensity, as discussed earlier. For convergence, residual type of RMS and the residual target value of 1×10^{-6} were set as the criteria.

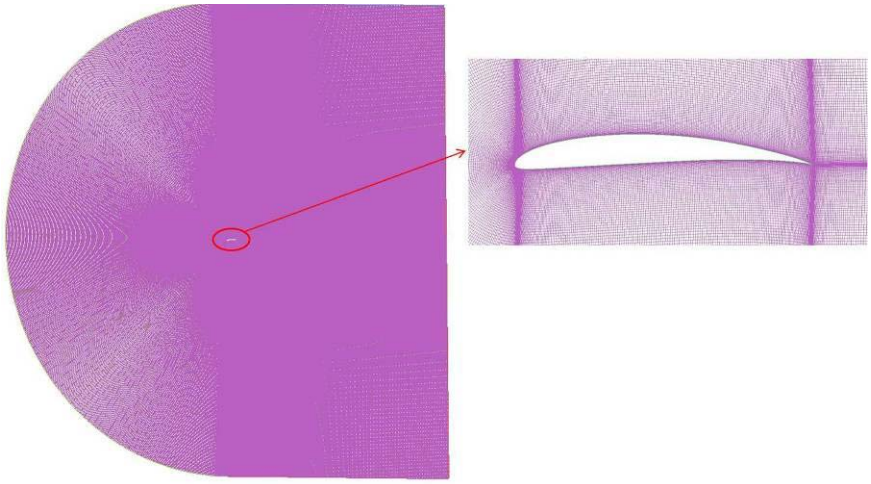

Fig. 2. Meshing around the airfoil.

4. Results and Discussion

4.1 Effect of Reynolds number

The results are presented and discussed in this section. For the calculation of C_P the measured static pressure at a point was non-dimensionalized with respect to the freestream static pressure and the corrected freestream velocity.

Figure 3 shows a comparison of numerical and experimental values of Cp for $\alpha = 0^o$ and Re = 100,000. The freestream turbulence level was 1% in this case. It can be seen that the experimental values of the pressure coefficient on the upper surface are slightly higher (lower suction) compared to the numerical values. However, overall, there is a good agreement between the experimental and numerical values. The lift and drag coefficients were obtained from the measured values of lift and drag forces, corrected for blockage effects as per the procedure described by Barlow et al. [15] as well as from numerical calculations.

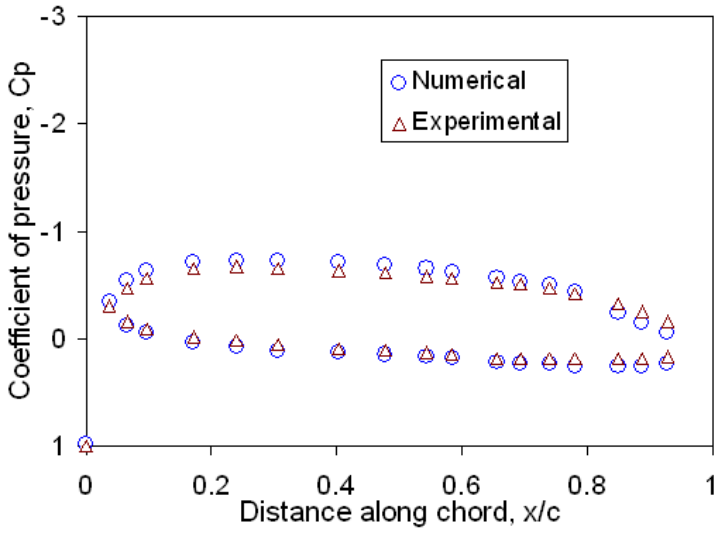

Fig. 3. Comparison of numerical and experimental pressure distributions on the airfoil surface for $\alpha = 0^o$, Re = 100,000 and Tu = 1%.

The pressure distributions, obtained experimentally on the surface of the airfoil for $\alpha = 4^o$ at the four Re values of 38,000, 100,000, 150,000 and 200,000 are presented in Fig. 4. The suction on the upper surface increases to a good extent from Re = 38,000 to Re = 150,000 and then to a smaller extent when Re is increased to 200,000.

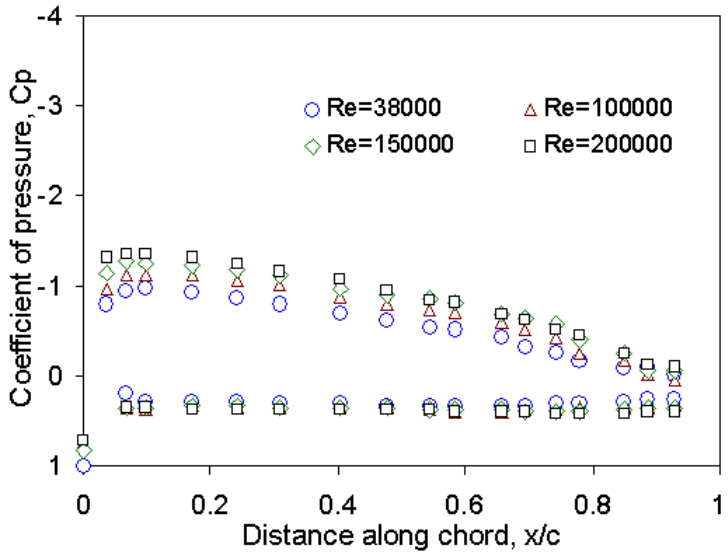

Fig. 4. Pressure distributions on the airfoil surface for $\alpha = 4^o$ at different Re and Tu = 1%.

The pressure on the lower surface and the suction effect on the upper surface increase with angle of attack. The experimental pressure distributions for $\alpha = 10^o$ and the four Re are shown in Fig. 5. The stagnation point that was at the leading edge of the airfoil (Cp values close to 1.0 at x/c = 0) for $\alpha = 4^o$ has moved down to the lower surface resulting in suction at the leading edge (negative Cp values at x/c = 0). The stagnation point was located at about x/c = 0.015 for Re = 150,000 as per the numerical results. The minimum value of Cp (obtained numerically) for this case is about -3.1; however, it could not be recorded experimentally because of the distance of the first pressure tap from the leading edge. The pressure on the lower surface as well as the suction on the upper surface increase with Re.

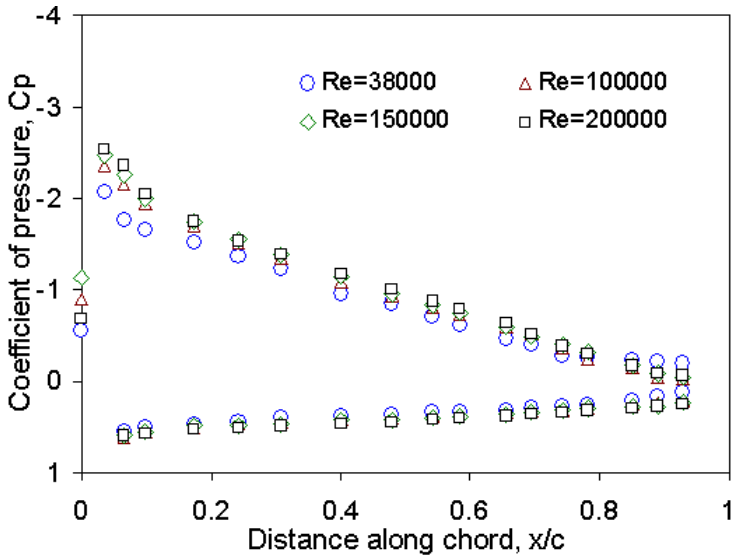

Fig. 5. Pressure distributions on the airfoil surface for $\alpha = 10^o$ at different Re and Tu = 1%

Additional information on the flow characteristics was obtained from numerical calculations, where required. The streamline pattern on the airfoil surface was obtained for different cases to study the flow in detail. Figure 6 shows the streamlines around the airfoil for $\alpha = 10^o$ and Re = 150,000, obtained using CFX. The deceleration of the flow on the lower surface and the acceleration of the flow on the upper surface can be seen from the figure. The velocity on the upper surface close to the leading edge is twice that of the freestream velocity, providing the higher pressure difference for the generation of lift. The flow was found to separate just before the trailing edge from the upper surface, as it decelerated while overcoming the adverse pressure gradient towards the trailing edge.

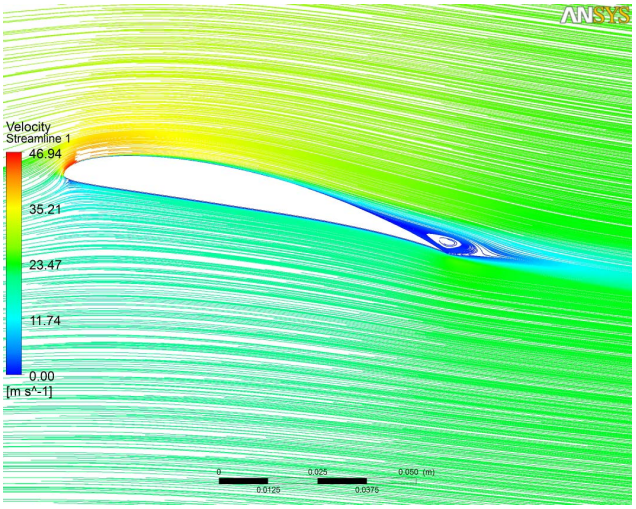

Fig. 6. Streamlines around the airfoil for $\alpha = 10^o$, Re = 150,000 and Tu = 1%.

The turbulent kinetic energy per unit mass was estimated using the relation

$$T.K.E. = \frac{1}{2}(\overline{u'^2} + \overline{v'^2})$$

Information on the location of transition on the upper surface was also obtained to study the contributions of pressure drag and friction drag at different angles of attack and at different freestream turbulence intensities (Tu). Figure 7 shows the turbulent kinetic energy around the airfoil for $\alpha = 10^o$ and Re = 150,000 obtained using CFX. The location of transition on the upper surface was at about 0.09c from the leading edge for this case. The growth of the turbulent boundary layer and turbulent kinetic energy over the airfoil and in the wake region can be seen in this figure.

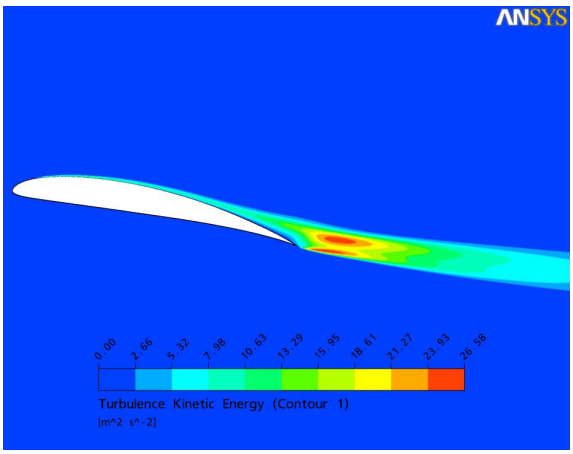

Fig. 7. Turbulent kinetic energy around the airfoil and in the wake region for $\alpha = 10^o$, Re = 150,000 and Tu = 1%.

The variations of the coefficient of lift with angle of attack for three Re are shown in Fig. 8. The lift and drag coefficients were calculated from the measured lift and drag values. The lift coefficient is found to increase continuously up to 14° for the lowest Re of 38,000 after which it starts to decrease due to the separation of the flow from the upper surface. For the Re of 100,000 and above, the coefficient of lift increases up to 16° and then starts to decrease beyond this angle. It is interesting to note that the drop in the C_l values is gradual, as the point of separation moves upstream. The highest values of C_l were recorded for the Re of 200,000. For this Re, the value of C_l dropped only a little from 16° to 18°, indicating that the stall for this airfoil is not sudden. A number of NACA airfoils exhibit an abrupt cut off in the lift coefficient, making those airfoils unsuitable for wind turbine applications where the flow angle can change suddenly and the turbine is still expected to generate sufficient lift force. It is also interesting to note that no hysteresis was observed till the highest angle investigated in this case. It should be noted that the freestream turbulence level was not very low in the present work. For this particular case, it was about 1%.

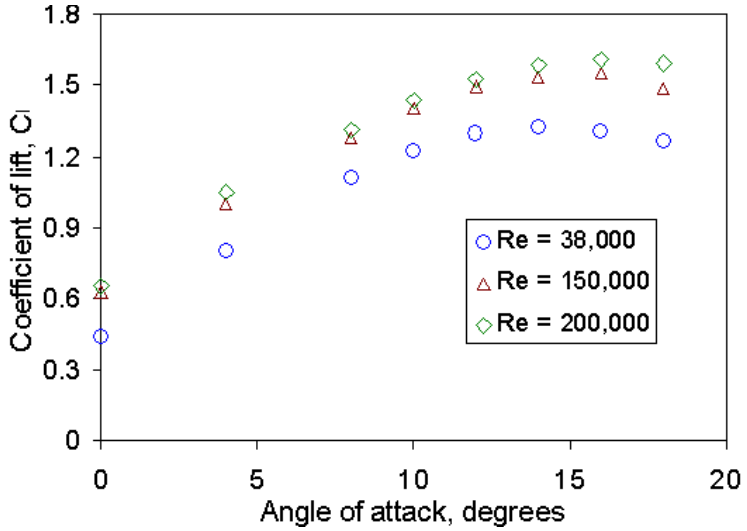

Fig. 8. Variation of the coefficient of lift with angle of attack for different Re at Tu = 1%.

The variations of the coefficient of drag with angle of attack for the three Re are shown in Fig. 9. The drag force increases slowly with angle of attack for lower angles; from the angle of 14° for Re = 38,000 and of 16° for Re = 150,000 there is a significant increase in the drag coefficient, indicating the onset of stalling process.

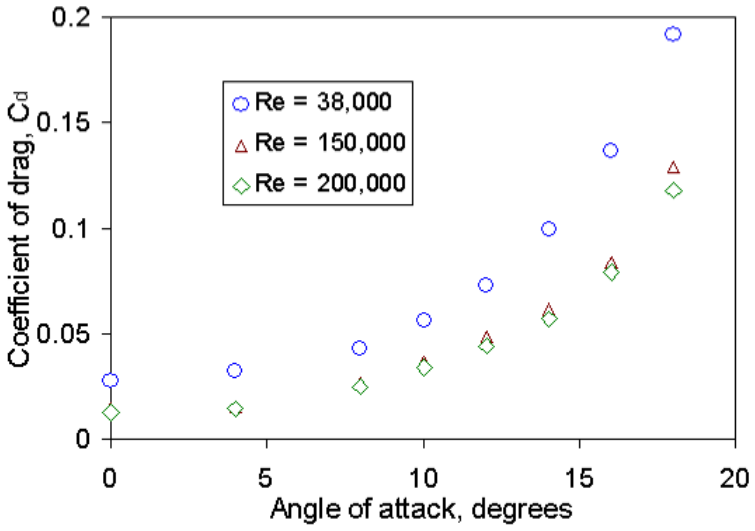

Fig. 9. Variation of the coefficient of drag with angle of attack for different Re at Tu = 1%.

4.2 Effect of freestream turbulence intensity

When the value of Tu is increased from the 1% level to 5% and 10%, the location of transition on the upper surface was found to shift upstream. The distance of the transition point from the leading edge for higher turbulence intensities reduced significantly compared to Tu = 1% for smaller angle of attack. The turbulence kinetic energy for $\alpha = 4^o$ and Tu = 10% at Re = 150,000, obtained with CFX, is shown in Fig. 10. This Re was chosen for a detailed investigation because it is expected that the airfoil will perform better at higher Re of 200,000 or higher if it performs well at Re = 150,000. The location of transition has moved significantly upstream compared to the case when Tu = 1% (not shown). As the transition point moves upstream, the region of laminar boundary layer reduces and the region of turbulent boundary layer increases. As a result, a larger region of turbulent boundary layer can be seen from this figure. For a given angle of attack, this results in an increase in the skin friction drag. The skin friction component of the drag is estimated using $C_{df} = \oint C_f \, d\bar{x}$ where C_f is the skin friction coefficient [16].

The pressure drag normally reduces as the point of separation moves downstream towards the trailing edge.

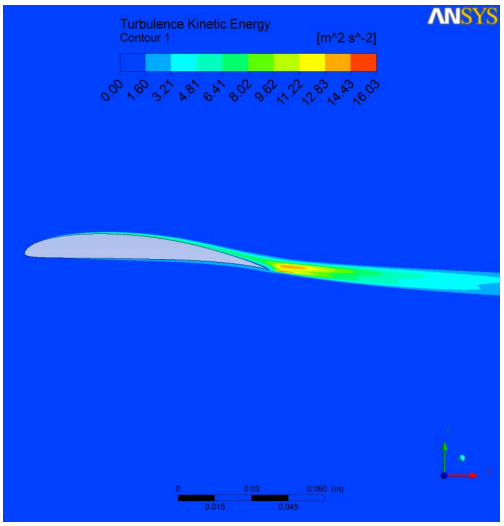

Fig. 10. Turbulence kinetic energy around the airfoil and in the wake region for $\alpha = 4^o$, Re = 150,000 and Tu = 10%.

The locations on the upper surface where transition to the turbulent boundary layer took place for Re = 150,000 at different angles of attack and the three turbulence levels are shown in Fig. 11. For all the angles of attack, the location of transition can be seen to be moving upstream with increasing turbulence level. For the angle of attack of 4^o, the location of transition moved considerably upstream with increasing turbulence levels of the incident flow. For the higher angles of 14^o and above, the shift is not much because the transition point is already close to the leading edge. This has the advantage of not altering the flow structure over the upper surface when the turbine blade leading edge gathers dust and dirt etc. resulting in tripping of the boundary layer. In fact, many turbine blade designers (e.g. Ref. [17]) choose a design angle of attack which has the transition point close to the leading edge for this reason.

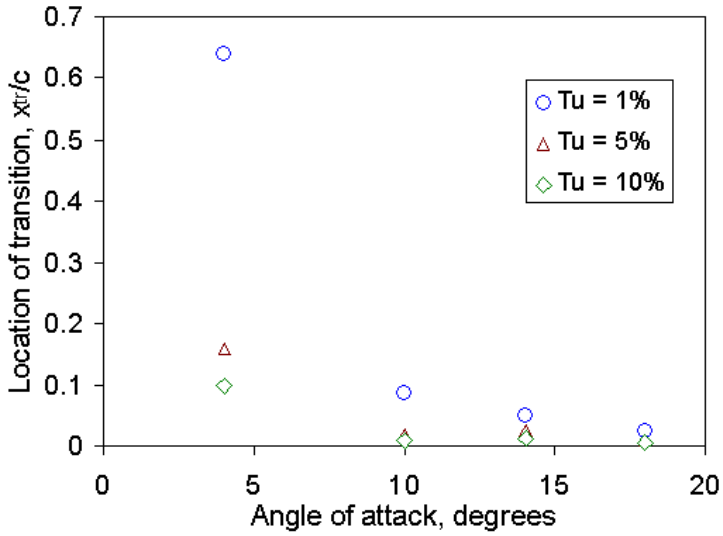

Fig. 11. Locations of transition on the upper surface for Re = 150,000 at different angles of attack and turbulence levels.

The pressure distributions on the airfoil surface for $\alpha = 14^{o}$, Re = 150,000 and the three trubulence levels of the incident flow, obtained experimentally, are shown in Fig. 12. A comparison of this figure with Fig. 5 shows that there is a kink in the pressure distribution at about x/c = 0.1 indicating the transition of the boundary layer to turbulent; however, in Fig. 12, the transition has already occurred before the first pressure tap (Fig. 11). It is interesting to observe that the suction on the upper surface is higher for higher turbulence level. Although enhanced suction is always desirable to get higher lift, it also means greater deceleration towards the rear. For any type of trailing edge, the flow decelerates to below freestream values. If the deceleration is too severe, separation occurs. However, in this case, the separation is occurring for the lower suction case because the freestream turbulence level is the lowest for this case. At higher turbulence level of the incident flow, the energy transfer between the external flow and the boundary layer increases since a part of the incident flow's turbulent kinetic energy is transferred to the flow in the boundary layer, which has the effect of increasing its resistance to separation [11]. It is also interesting to observe that the pressure on the lower surface is slightly higher for the case of higher freestream turbulence level. The stagnation point was located at about x/c = 0.03 (obtained numerically) for Tu = 5% for this case. Close to the trailing edge, where the flow is separated on the upper surface at the lowest turbulence level, the pressure on the lower surface also reduces to match the pressure at the trailing edge. For the case of the highest turbulence level of 10%, the pressure on the upper surface continuously increases till the trailing edge indicating that the flow is attached to the surface. This will result in a higher lift coefficient, as will be discussed later. Similar observations were made by Swalwell et al. [10], Devinant et al. [11] and Maeda et al. [12] who found that the point of separation moves downstream for higher freestream turbulence intensities. Since the boundary layer is turbulent almost throughout the upper surface for this angle (Fig. 11), the higher suction on the upper surface for the case of higher turbulence intensity indicates higher turbulent mean velocity. It is known that for a given type of boundary layer, a higher mean velocity reduces the skin friction drag [1,16]. At the same time, the pressure drag reduces because the separation point moves downstream resulting in a thinner wake and a lower momentum loss.

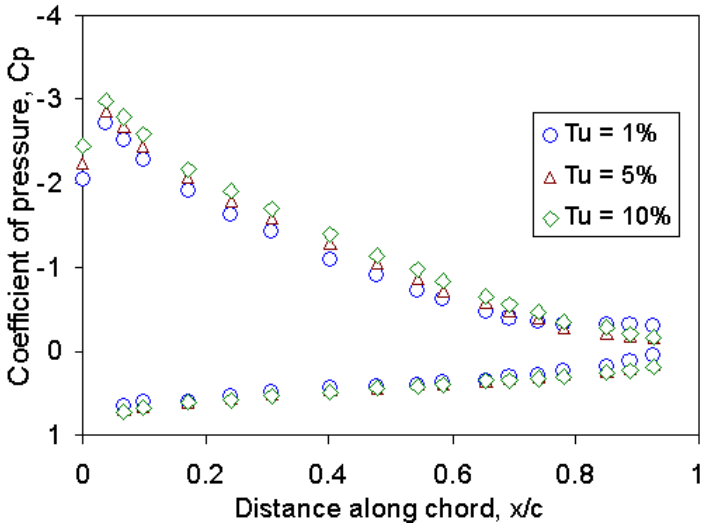

Fig. 12. Pressure distributions on the airfoil surface for $\alpha = 14^{o}$ at Re = 150,000 and different turbulence levels.

The turbulent kinetic energy for the case of $\alpha = 14^{o}$, Re = 150,000 and Tu = 10% is shown in Fig. 13. The nearly fully turbulent flow region and higher levels of turbulence intensity on the upper surface compared to lower angle of attack (Fig. 10) or a lower freestream turbulence intensity (Fig. 7) can clearly be seen from this figure.

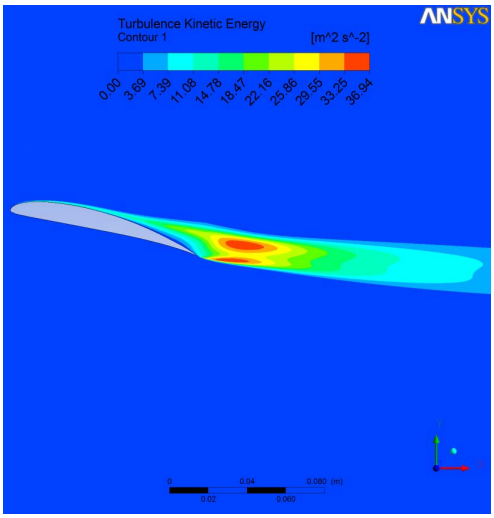

Fig. 13. Turbulent kinetic energy for $\alpha = 14^{o}$, Re = 150,000 and Tu = 10%.

The streamlines around the airfoil for $\alpha = 16^{o}$, Re = 150,000 and Tu = 10% are shown in Fig. 14. The much higher acceleration of the flow over the upper surface resulted in a velocity increase of nearly 150% compared to the freestream near the leading edge (suction peak). This corresponds to a pressure coefficient of -5 which was the value recorded in CFX computations. The point of separation for this case was observed to be slightly aft of the mid-chord point. The separated flow has a large vortex, which is bigger in size compared to the lower angle of attack of 10^{o} (Fig. 6). It is also interesting to observe that there is a bigger area of nearly stagnant flow on the lower surface compared to the angle of attack of 10^{o}. This contributes to higher values of Cp on the lower surface.

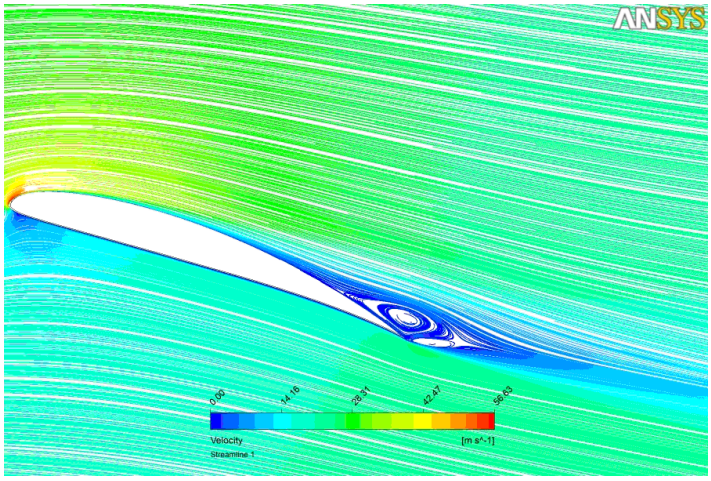

Fig. 14. Streamlines around the airfoil for $\alpha = 16^{o}$, Re = 150,000 and Tu = 10%.

The experimental pressure distributions on the airfoil surface for $\alpha = 18^{o}$ at Re = 150,000 and different turbulence levels are shown in Fig. 15. A detailed study of this figure makes an interesting reading – for the lowest value of freestream turbulence intensity, the flow separates from the upper surface quite early, approximately after the mid-chord point. When the turbulence intensity is increased, the point of separation moves downstream. This is due to the higher energy in the turbulent external flow that transfers energy to the boundary layer, as discussed earlier. For the highest turbulence intensity, the flow remains attached to the upper surface for a much larger length of the airfoil.

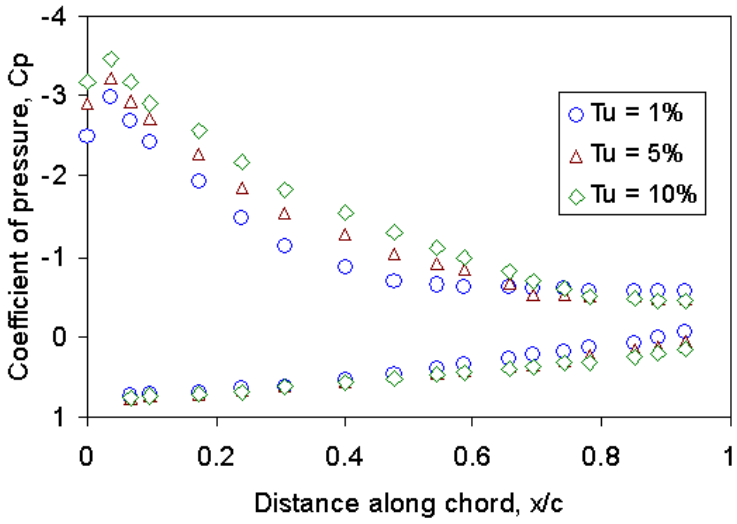

Fig. 15. Pressure distributions on the airfoil surface for $\alpha = 18^{o}$ at Re = 150,000 and different turbulence levels.

Figure 16 shows the values of C_l for Re = 150,000 at the three turbulence levels. It is interesting to observe that the lift coefficient is lower at angles of attack up to 10^{o} for the higher turbulence intensities. From Fig. 11, it is clear that till an angle of attack of 10^{o}, the upstream shift of the transition point on the upper surface increases the region of turbulent boundary layer and the resulting higher skin friction causes a smaller pressure recovery than the case with a reduced turbulent boundary layer region; this results in a slight drop in the lift coefficient as can be seen from the figure. For the angles of attack of 12^{o} and above, there is no significant shift in the location of transition with increasing turbulence intensity; however, the energy transfer from the external flow to the boundary layer increases which energizes the boundary layer and increases its resistance to flow separation. As a result, the

boundary layer remains attached to the upper surface till very close to the trailing edge, as can be seen from the pressure distributions in Fig. 12 and Fig. 15. The delayed separation results in a higher lift coefficient for the higher angles, shown in Fig. 16.

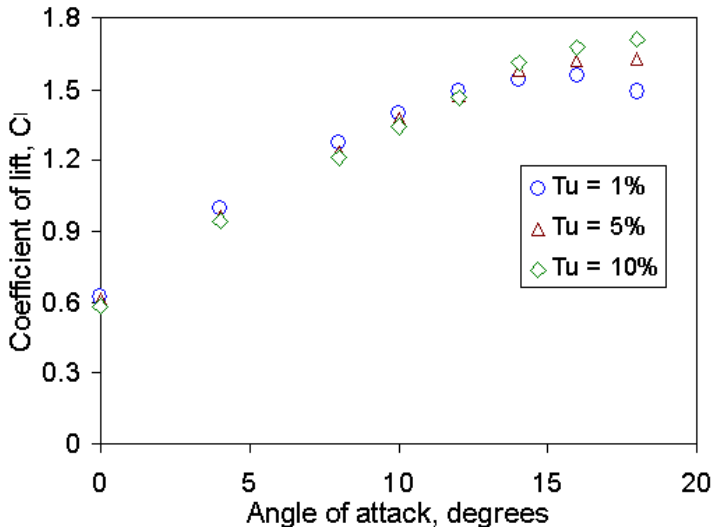

Fig. 16. Variation of the coefficient of lift with angle of attack at Re = 150,000 for different turbulence levels.

The variations of the drag coefficient with angle of attack at Re = 150,000 corresponding to different turbulence intensities are shown in Fig. 17. As discussed earlier, for lower angles of attack, the location of transition moves upstream for higher turbulence levels, which increases the region of turbulent boundary layer hence increasing the skin friction drag. The pressure drag does not change much because for lower angles, the flow remains attached to the upper surface till the trailing edge or very close to it even at low freestream turbulence levels. For the case of 0^o angle of attack, it was expected that the drag will be much higher at Tu = 10% compared to the case of Tu = 1%; however, there was only a small increase in C_d for both 0^o and 4^o cases.

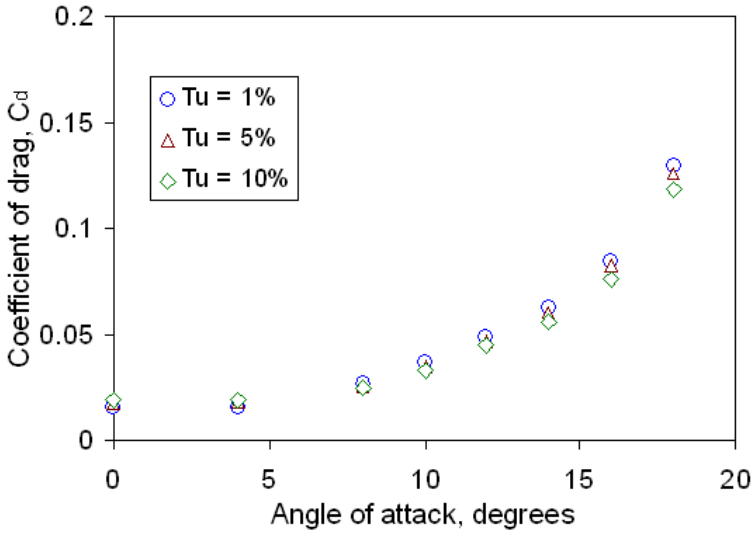

Fig. 17. Variation of the coefficient of drag with angle of attack at Re = 150,000 for different turbulence levels.

For the higher angles of attack, the downstream shift of the point of separation results in a thinner wake and a lower momentum loss, resulting in a lesser drag. Also, as discussed earlier, for a given type of boundary layer, a higher mean velocity results in a lower skin

friction drag. Both these components cause a greater reduction in the total drag of the airfoil for higher angles of attack, as can be seen from Fig. 17. As a result of increasing the freestream turbulence level from 1% to 10%, the lift to drag ratio increased by 8% to 15% in the α-range of interest of 10^o to 14^o from which the design angle of attack can be chosen after considering other parameters involved. Experiments conducted in the past (e.g. Ref. [18]) at 70% of the blade length from the hub have shown that the pressure distributions for the pre-stall and stall flow conditions for the rotating and stationary blade are almost identical and resemble those commonly observed on two-dimensional airfoils near stall. As the region under focus in the present work is also at about the same distance from the hub, it is expected that the performance of the actual rotating blade will be similar to what is observed in the present work.

5. Conclusions

The aerodynamic characteristics of SG6043 airfoil are studied both experimentally and numerically at Reynolds numbers ranging from 38,000 to 200,000, angles of attack from 0^o to 20^o and freestream turbulence levels of 1%, 5% and 10%. The important conclusions from the present work are:

1. With increasing Reynolds number, the pressure on the lower surface and the suction on the upper surface increase, resulting in higher lift coefficients and lower drag coefficients.
2. At the lower turbulence intensity of 1%, the stalling occurs at 14^o for Re = 38,000 and at 16^o for Re = 150,000 and above. When the angle of attack is increased further, the lift coefficient drops only a little indicating that the stalling process is not abrupt for this airfoil.
3. At an angle of attack of 18^o at which the lift coefficient dropped from the 16^o value for the turbulence intensity of 1%, it increased when the turbulence intensity was increased to 10%.
4. When the freestream turbulence intensity is increased, the location of transition on the upper surface shifts upstream. This shift is significant for smaller angles of attack because transition at lower turbulence intensities occurs away from the leading edge. This shift causes an increase in the skin friction component of the drag, which is the major component of the total drag at small angles of attack.
5. A higher suction was recorded on the upper surface for higher angles for the case of higher turbulence intensities indicating higher turbulent mean velocity. It is known that for a given type of boundary layer, a higher mean velocity reduces the skin friction drag. At the same time, the pressure drag reduces because the separation point moves downstream resulting in a thinner wake and a lower momentum loss.
6. The lift to drag ratio increased by 8% to 15% as a result of increasing the turbulence level from 1% to 10% between angles of attack of 10^o and 14^o.
7. It is advisable to choose a profile that has the upper surface transition point very close to the leading edge at the design angle of attack, so that the performance does not get affected when the turbulence level changes or the leading edge gather dirt, dust etc. For SG6043, it will be best to choose an angle of attack between 10^o and 14^o.

References

1. Abbott, I. H. and Van Doenhaff, A. E., *Theory of Wing Sections,* Dover Publications Inc., New York (1958), p. 100, pp. 452-687 .
2. Fupeng, H., Yuhong, L. and Zuoyi, C., "Suggestions for Improving Wind Turbines Blade Characteristics," *Wind Engineering*, Vol. 25 (2001), pp. 105-113.
3. Xuan, H., Weimin, Z., Xiao, L. and Jieping, L. "Aerodynamic and Aeroacoustic Optimization of Wind Turbine Blade by a Genetic Algorithm," *Proceedings of 46th AIAA Aerospace Sciences Meeting and Exhibit* (2008), Reno, Nevada, AIAA-2008-1331.

4. Selig, M. S. and McGranahan, B. D., "Wind Tunnel Aerodynamic Tests of Six Airfoils for Use on Small Wind Turbines, *NREL Report SR-500-34515* (2004).
5. Giguerre, P. and Selig, M. S., "Low Reynolds Number Airfoils for Small Horizontal Axis Wind Turbines," *Wind Engineering*, 21 (1997), pp. 367-380.
6. Drela, M., "XFOIL: an analysis and design system for low Re airfoils," *Conference on Low Re Airfoil Aerodynamics*, University of Notre Dame (1989).
7. Selig, M. S. *UIUC Airfoil Data Site:* www.ae.illinois.edu/m-selig/ads.html.
8. *Airfoil Investigation Database*, online at http://www.worldofkrauss.com/foils/787
9. Hoffmann, J. A., "Effect of Freestream Turbulence on the Performance Characteristics of an Airfoil," *AIAA Journal*, 29 (1991), pp. 1353-1356.
10. Swalwell, K. E., Sheridan, J. and Melbourne, W. H., "The Effect of Turbulence Intensity on Stall of the NACA 0021 Aerofoil," *Proc. 14th Australasia Fluid Mechanics Conference*, Adelaide, (2001), pp. 941-944.
11. Devinant, Ph. Laverne, T., Hureau, J., "Experimental Study of Wind-Turbine Airfoil Aerodynamics in High Turbulence," *Journal of Wind Engineering and Industrial Aerodynamics*, 90 (2002), pp. 689-707.
12. Maeda, T., Kamada, Y., Murata, J., Toki, T. and Tobuchi, A., "Effect of Turbulence Intensity on Dynamic Characteristics of Wind Turbine Airfoil," *Proc. of RE2010 Conference* (2010), Paper No. P-Wd-36.
13. Sicot, S., Devinant, P., Laverne, T., Loyer, S. and Hureau, J., "Experimental Study of the Effect of Turbulence on Horizontal Axis Wind Turbines," *Wind Energy*, 9 (2006), pp. 361-370.
14. Garratt, J. R. and Taylor, P. A., *Boundary-Layer Metereology*, Kluwer Academic Publishers, Netherlands (1996), pp. 300-318.
15. Barlow, J. B., Rae, W. H. Jr., Pope, A., *Low Speed Wind Tunnel Testing*, Wiley Interscience, New York (1999), pp. 349-363.
16. White, F. M., *Viscous Fluid Flow*, McGraw Hill, New York (2006), p. 235, pp. 433-438.
17. Fuglsang, P., Bak, C., Gaunaa, M. and Antoniou, I., "Design and Verification of the RisØ-B1 Airfoil Family for Wind Turbines," *ASME Journal of Solar Energy Engineering*, 126 (2004), pp. 1002-1010.
18. Maeda, T., Ismaili, E., Kawabuchi, H. and Kamada, Y., "Surface Pressure Distribution on a Blade of a 10 m Diameter HAWT (Field Measurements versus Wind Tunnel Measurements)," *ASME Journal of Solar Energy Engineering*, 127 (2005), pp. 185-191.